

# A public database for white dwarf asteroseismology with fully evolutionary models

## I. Chemical profiles and pulsation periods of ZZ Ceti (DAV) stars

Alejandra D. Romero<sup>1,2</sup>, Alejandro H. Córscico<sup>1,2</sup>, Leandro G. Althaus<sup>1,2</sup>, & Marcelo M. Miller Bertolami<sup>1,2</sup>

<sup>1</sup>*Facultad de Ciencias Astronómicas y Geofísicas, Universidad Nacional de La Plata, Paseo del Bosque s/n, (1900) La Plata, Argentina*

<sup>2</sup>*Consejo Nacional de Investigaciones Científicas y Técnicas (CONICET)*

Emails: aromero, acorsico, althaus, mmiller@fcaglp.unlp.edu.ar

**Abstract.** We present a large bank of chemical profiles and pulsation periods suited for asteroseismological studies of ZZ Ceti (or DAV) variable stars. Our background equilibrium DA white dwarf models are the result of fully evolutionary computations that take into account the complete history of the progenitor stars from the ZAMS. The models are characterized by self-consistent chemical structures from the centre to the surface, and cover a wide range of stellar masses, effective temperatures, and H envelope thicknesses. We present dipole and quadrupole pulsation  $g$ -mode periods comfortably covering the interval of periods observed in ZZ Ceti stars.

Complete tabulations of chemical profiles and pulsation periods to be used in asteroseismological period fits, as well as other quantities of interest, can be freely downloaded from our website (<http://www.fcaglp.unlp.edu.ar/evolgroup>).

## 1. Introduction

White dwarf asteroseismology is a powerful astrophysical tool that fully exploits the comparison between the observed pulsation periods in white dwarfs and the periods computed for appropriate theoretical models. It allows us to infer details of the origin, internal structure and evolution of white dwarfs (Winget & Kepler 2008; Althaus et al. 2010a). ZZ Ceti (or DAV) stars constitute the most numerous group of degenerate variable stars. They are otherwise normal DA (H-rich atmospheres) white dwarfs that exhibit  $g$ (gravity)-mode pulsations. Recently, our group **La Plata Stellar Evolution and Pulsation Research Group** has performed for the first time a detailed asteroseismological study on an ensemble of 44 bright ZZ Ceti stars by employing fully evolutionary (that is, non static) DA white dwarf models (Romero et al. 2012, Romero 2012). Our asteroseismological approach basically consists in the employment of a large suite of detailed stellar models characterized by very accurate and updated physical ingredients. These models were produced by computing the complete evolution of the progenitor stars. We have applied successfully this approach to the hot GW Vir (or DOV) stars in the past (see Córscico et al. 2007a, 2007b, 2008, 2009). Since the final

chemical stratification of white dwarfs is fixed in prior stages of their evolution, the evolutionary history of progenitor stars is of utmost importance in the context of white dwarf asteroseismology.

Here, we present a complete set of pulsational results that can be useful to perform asteroseismological studies of ZZ Ceti stars. These include the internal chemical profiles and the run of the Brunt-Väisälä and Lamb frequencies, as well as a large set of adiabatic pulsation periods, time-averaged oscillation kinetic energies, and first order rotational splitting coefficients. All these quantities can be freely downloaded from our website.

This database can be used in two ways: (1) carrying out period fits using directly the bank of periods we provide, corresponding to our set of equilibrium DA white dwarf models, or alternatively, (2) by scaling our internal chemical profiles to the structure of other independent DA white dwarf models, and then by performing period fits using the pulsation periods computed for such models.

Below, we summarily describe the input physics of our models and the pulsation computations, and then we present the format of our database.

## 2. Input physics and evolutionary computations

The state-of-the-art DA white dwarfs evolutionary models employed have been computed with the LPCODE evolutionary code. Details of this code and the input physics that this code includes can be found in Althaus et al. (2010b), Renedo et al. (2010) and references therein. Below, we briefly enumerate the main physical ingredients:

- For the high-density regime characteristics of white dwarfs, we have used the equation of state (EoS) of Segretain et al. (1994).
- For the low-density regime, we used an updated version of the EoS of Magni & Mazzitelli (1979).
- Radiative opacities are from the OPAL project (Iglesias & Rogers 1996), including carbon- and oxygen-rich composition, supplemented at low temperatures with the molecular opacities of Alexander & Ferguson (1994).
- Conductive opacities are those of Cassisi et al. (2007).
- Neutrino emission rates are taken from Itoh et al. (1996) and Haft et al. (1994).
- The  $^{12}\text{C}(\alpha, \gamma)^{16}\text{O}$  reaction rate, of special relevance for the C-O stratification of the white dwarf, is that of Angulo et al. (1999).
- Convection has been modeled with the formalism of the mixing-length theory as given by the ML2 parametrization (Tassoul et al. 1990).
- Treatment of the chemical profiles. We have considered the distinct physical processes that are responsible for changes in the chemical abundance distribution during white dwarf evolution:
  - Element diffusion: it strongly modifies the chemical composition profile throughout their outer layers. We have considered gravitational settling as

well as thermal and chemical diffusion of  $^1\text{H}$ ,  $^3\text{He}$ ,  $^4\text{He}$ ,  $^{12}\text{C}$ ,  $^{13}\text{C}$ ,  $^{14}\text{N}$ , and  $^{16}\text{O}$ . The treatment of time-dependent diffusion is based on the multicomponent gas treatment presented in Burgers (1969). Diffusion becomes operative once the wind limit is reached at high effective temperatures (Unglaub & Bues 2000). As shown in previous studies, diffusion in the white dwarf envelope is a key ingredient as far as the mode-trapping properties of ZZ Ceti stars is concerned.

- Abundance changes resulting from residual nuclear burning (mostly during the hot stages of white dwarf evolution) have been taken into account. Nuclear burning fixes the maximum value of  $M_{\text{H}}$  that is expected in a DA white dwarf.
- Chemical re-homogenization of the inner carbon-oxygen profile induced by Rayleigh-Taylor instabilities has been considered following Salaris et al. (1997). These instabilities arise because of the positive molecular weight gradients that remain above the flat chemical profile left by convection during core helium burning.

### 3. Pulsation computations

We have employed the pulsation code described in Córscico & Althaus (2006), which is coupled to the LPCODE evolutionary code. The pulsation code is based on a general Newton-Raphson technique that solves the full fourth-order set of equations governing linear, adiabatic, nonradial stellar pulsations following the dimensionless formulation of Dziembowski (1971) (see Unno et al. 1989). The pulsation code provides the dimensionless eigenfrequency  $\omega_k$  ( $k$  being the radial order of the mode) and eigenfunctions  $y_1, \dots, y_4$ . From these basic quantities, the code computes pulsation periods ( $\Pi_k$ ), time-averaged oscillation kinetic energies ( $E_k$ ), rotation splitting coefficients ( $C_k$ ), weight functions ( $W_k$ ), and variational periods ( $\Pi_k^{\text{v}}$ ) for each computed eigenmode (see Appendix A of Córscico & Althaus 2006 for the definition of these quantities). Usually, the relative difference between  $\Pi_k^{\text{v}}$  and  $\Pi_k$  is lower than  $\approx 10^{-4}$ , which represents the typical uncertainties in our theoretical periods. The prescription we follow to assess the run of the Brunt-Väisälä frequency ( $N$ ) for a degenerate environment typical of the deep interior of a white dwarf is the so-called “Ledoux Modified” treatment (Tassoul et al. 1990), appropriately generalized to include the effects of having three nuclear species (oxygen, carbon, and helium) varying in abundance in the same place of the star (a triple chemical interface). Fig. 1 displays an example of the chemical profiles of our models with a fixed stellar mass and effective temperature and for different thicknesses of the H envelope (upper panel), and the run of the Brunt-Väisälä and Lamb (for  $\ell = 1$ ) frequencies (lower panel). Details can be found in Romero et al. (2012) and Romero (2012).

We present results for DA white dwarf models with stellar masses, effective temperatures and H envelope thicknesses in the ranges  $0.525 \leq M_*/M_{\odot} \leq 0.878$ ,  $9000 \leq T_{\text{eff}} \leq 14000$  K, and  $-3.62 \leq \log(M_{\text{H}}/M_*) \leq -9.34$ , respectively. We have performed pulsation calculations on about  $(11 \times 7 \times 200) = 15400$  DA white dwarf models. In this account, we have considered the number of stellar mass values (11), the number of thicknesses of the H envelope for each sequence ( $\approx 7$ ), and the number of models ( $\approx 200$ ) with effective temperature in the interval  $14000 - 9000$  K, respectively. For each model, adiabatic pulsation  $g$ -modes with  $\ell = 1$  and 2 and periods in the range

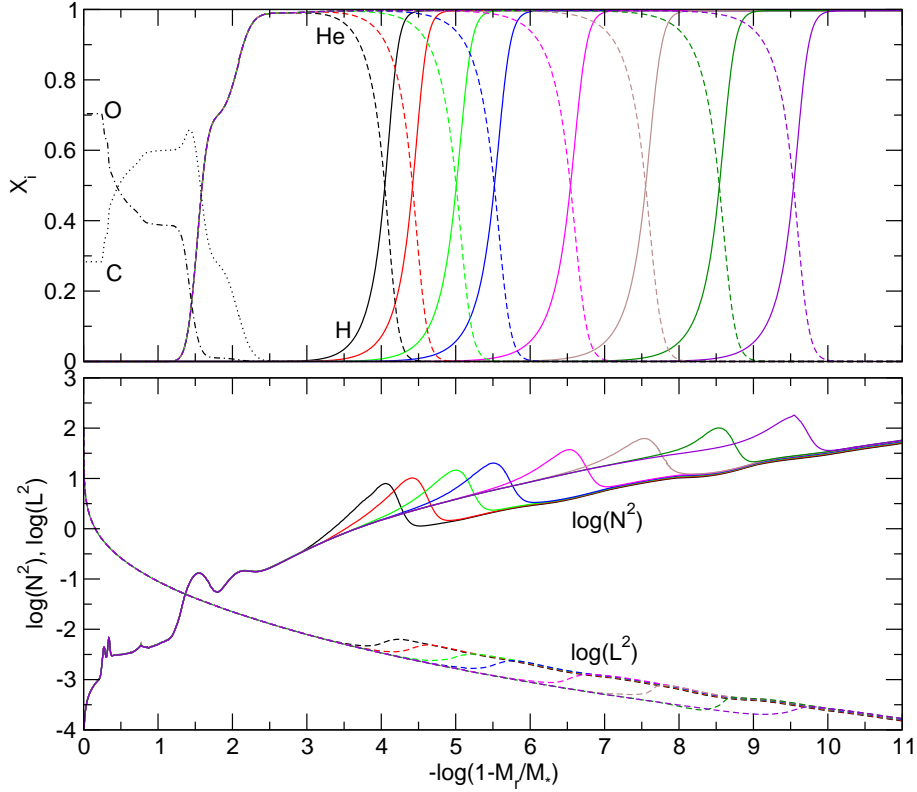


Figure 1. Upper panel: example of the internal chemical profiles for  $^1\text{H}$ ,  $^4\text{He}$ ,  $^{12}\text{C}$ , and  $^{16}\text{O}$  of our DA white dwarf models. The cases shown in the figure correspond to models with a stellar mass of  $M_* = 0.593M_\odot$ , an effective temperature of  $T_{\text{eff}} \sim 12\,350$  K, and H envelope thicknesses of  $\log(M_{\text{H}}/M_*) = -3.93$  (black),  $-4.28$  (red),  $-4.85$  (green),  $-5.34$  (blue),  $-6.33$  (magenta),  $-7.34$  (brown),  $-8.33$  (dark green), and  $-9.33$  (violet). Lower panel: the logarithm of the squared Brunt-Väisälä and Lamb frequencies corresponding to the cases depicted in the upper panel. The correspondence between each bump-like feature in  $N^2$  and the chemical transition regions of the models is clearly visible.

80 – 2000 s have been computed. This range of periods corresponds (on average) to  $1 \lesssim k \lesssim 50$  for  $\ell = 1$  and  $1 \lesssim k \lesssim 90$  for  $\ell = 2$ . So, more than  $\sim 2 \times 10^6$  adiabatic pulsation periods have been computed. An example of our pulsation results is depicted in Fig. 2, where we show the forward period spacing, the oscillation kinetic energy, and the first order rotational splitting coefficients for the same models analyzed in Fig. 1. Note the gradual changes experienced by these quantities as we vary the value of the H envelope thickness.

In Table 1 we show the grid of evolutionary sequences included in our database. The values of the stellar mass of our set of DA white dwarf models are shown in the upper row. The masses of H corresponding to the different envelope thicknesses for each stellar mass are shown in rows 2 to 9. Row 2 corresponds to the maximum value of the thickness of the H envelope for each stellar mass according to our evolutionary

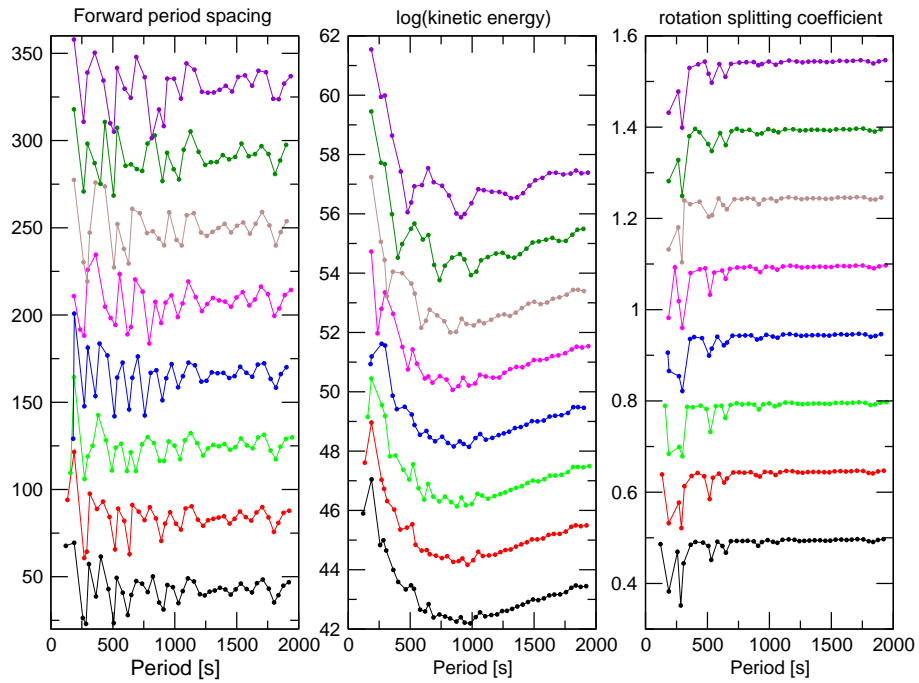


Figure 2. Pulsation quantities for  $\ell = 1$  modes corresponding to the same models analyzed in Fig. 1. In each panel, the curves have been arbitrarily shifted upwards for clarity, except the lowest one. Left panel: forward period spacing ( $\Delta\Pi_k = \Pi_{k+1} - \Pi_k$ ) vs periods; middle panel: oscillation kinetic energy ( $\log(E_k)$ ) vs periods; right panel: first order rotation splitting coefficient ( $C_k$ ) vs periods.

computations (“canonical envelopes”). Rows 3 to 9 correspond to H envelopes thinner than the canonical ones.

Table 1.

$M_*/M_\odot$	0.5249	0.5480	0.5701	0.5932	0.6096	0.6323	0.6598	0.7051	0.7670	0.8373	0.8779
$\log\left(\frac{M_H}{M_*}\right)$	-3.62	-3.74	-3.82	-3.93	-4.02	-4.12	-4.25	-4.45	-4.70	-5.00	-5.07
	-4.27	-4.27	-4.28	-4.28	-4.45	-4.46	-4.59				
	-4.85	-4.85	-4.84	-4.85	-4.85	-4.86	-4.87	-4.88	-4.91		
	-5.35	-5.35	-5.34	-5.34	-5.35	-5.35	-5.35	-5.36	-5.37	-5.41	-5.40
	-6.33	-6.35	-6.33	-6.33	-6.34	-6.34	-6.35	-6.35	-6.35	-6.36	-6.39
	-7.34	-7.33	-7.34	-7.34	-7.33	-7.35	-7.33	-7.35	-7.34	-7.36	-7.38
	-8.33	-8.33	-8.31	-8.33	-8.33	-8.33	-8.33	-8.34	-8.33	-8.34	-8.37
	-9.25	-9.22	-9.33	-9.33	-9.25	-9.34	-9.33	-9.34	-9.33	-9.34	-9.29

#### 4. Format of the files to be downloaded

The files of our database can be downloaded from our website:

[http://www.fcaglp.unlp.edu.ar/evolgroup/TRACKS/PULSATIONS/PULSATIONS\\_DA/pulsations\\_cocor](http://www.fcaglp.unlp.edu.ar/evolgroup/TRACKS/PULSATIONS/PULSATIONS_DA/pulsations_cocor)

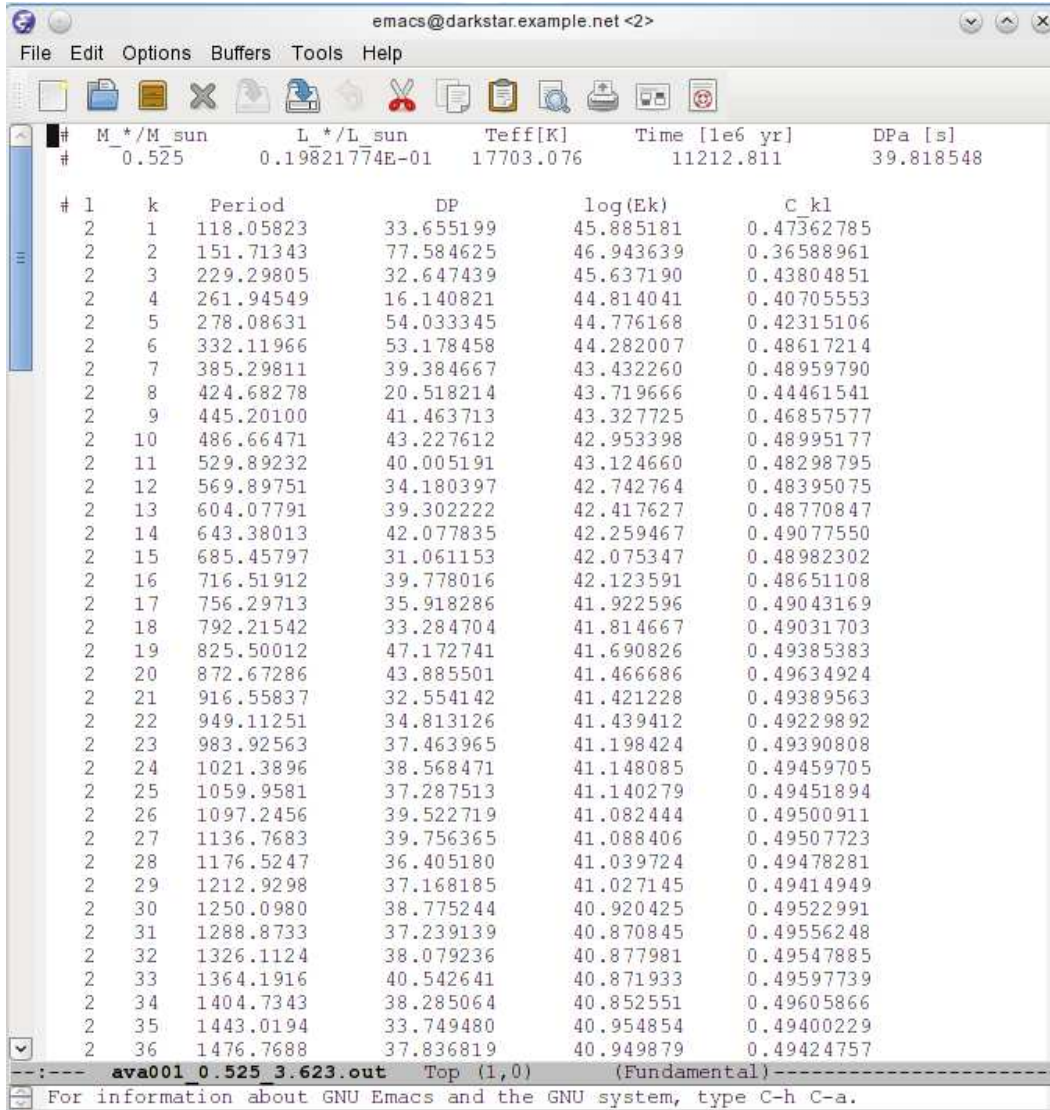
Once in the site, you can see that the files are organized in three separate tables, which have exactly the same form as Table 1 above. For a given table, each element is associated to a specific sequence characterized by the corresponding values of  $M_*$  and  $\log(M_H/M_*)$ . In the first table we provide results of periods ( $\Pi_k$ ) and the other quantities ( $\Delta\Pi_k$ ,  $\log(E_k)$  and  $C_k$ ) for the harmonic degree  $\ell = 1$ , in terms of the radial order  $k$ . The same information, but for the case  $\ell = 2$ , is provided in the second table. Finally, the third table includes the squared Brunt-Väisälä ( $N^2$ ) and Lamb ( $L_\ell^2$ ) frequencies, the Ledoux term ( $B$ ), and the chemical abundances (by mass) of hydrogen ( $X_H$ ), helium ( $X_{He}$ ), carbon ( $X_C$ ), and oxygen ( $X_O$ ) in terms of the radial coordinate ( $r/R_*$ ) and the outer mass fraction coordinate,  $[-\log(1 - M_r/M_*)]$ .

##### 4.1. The first table: periods and other quantities for $\ell = 1$

Each element of the table is a hyperlink that leads to a given tar gzipped file. You can download a specific tar gzipped file by simply clicking on a given element of the table. For instance, if you click at element [-3.62](#) in the first column of the table, you will download the file: `ava_0.525_3.623.tgz`. This file corresponds to the sequence with  $M_* = 0.525M_\odot$  and  $\log(M_H/M_*) = -3.623$ . After you detar the file, you should obtain a sequence of files:

```
ava001_0.525_3.623.out
ava002_0.525_3.623.out
ava003_0.525_3.623.out
ava004_0.525_3.623.out
⋮
```

Each of these files corresponds to a different, decreasing effective temperature. For instance, in Fig. 3 we show the appearance of the file `ava001_0.525_3.623.out`. The



#	k	Period	DP	log(Ek)	C_kl
#	M*/M_sun	L*/L_sun	Teff[K]	Time [1e6 yr]	DPa [s]
#	0.525	0.19821774E-01	17703.076	11212.811	39.818548
1	1	118.05823	33.655199	45.885181	0.47362785
2	2	151.71343	77.584625	46.943639	0.36588961
2	3	229.29805	32.647439	45.637190	0.43804851
2	4	261.94549	16.140821	44.814041	0.40705553
2	5	278.08631	54.033345	44.776168	0.42315106
2	6	332.11966	53.178458	44.282007	0.48617214
2	7	385.29811	39.384667	43.432260	0.48959790
2	8	424.68278	20.518214	43.719666	0.44461541
2	9	445.20100	41.463713	43.327725	0.46857577
2	10	486.66471	43.227612	42.953398	0.48995177
2	11	529.89232	40.005191	43.124660	0.48298795
2	12	569.89751	34.180397	42.742764	0.48395075
2	13	604.07791	39.302222	42.417627	0.48770847
2	14	643.38013	42.077835	42.259467	0.49077550
2	15	685.45797	31.061153	42.075347	0.48982302
2	16	716.51912	39.778016	42.123591	0.48651108
2	17	756.29713	35.918286	41.922596	0.49043169
2	18	792.21542	33.284704	41.814667	0.49031703
2	19	825.50012	47.172741	41.690826	0.49385383
2	20	872.67286	43.885501	41.466686	0.49634924
2	21	916.55837	32.554142	41.421228	0.49389563
2	22	949.11251	34.813126	41.439412	0.49229892
2	23	983.92563	37.463965	41.198424	0.49390808
2	24	1021.3896	38.568471	41.148085	0.49459705
2	25	1059.9581	37.287513	41.140279	0.49451894
2	26	1097.2456	39.522719	41.082444	0.49500911
2	27	1136.7683	39.756365	41.088406	0.49507723
2	28	1176.5247	36.405180	41.039724	0.49478281
2	29	1212.9298	37.168185	41.027145	0.49414949
2	30	1250.0980	38.775244	40.920425	0.49522991
2	31	1288.8733	37.239139	40.870845	0.49556248
2	32	1326.1124	38.079236	40.877981	0.49547885
2	33	1364.1916	40.542641	40.871933	0.49597739
2	34	1404.7343	38.285064	40.852551	0.49605866
2	35	1443.0194	33.749480	40.954854	0.49400229
2	36	1476.7688	37.836819	40.949879	0.49424757

---:--- **ava001\_0.525\_3.623.out** Top (1,0) (Fundamental) ---:---

For information about GNU Emacs and the GNU system, type C-h C-a.

Figure 3. The aspect of the file `ava001_0.525_3.623.out`, corresponding to a DA white dwarf model with  $M_* = 0.525M_\odot$ ,  $L_*/L_\odot = 1.9822 \times 10^{-2}$ ,  $T_{\text{eff}} = 17703$  K,  $\tau = 11212.811 \times 10^6$  yr, and  $\log(M_{\text{H}}/M_*) = -3.623$ .

heading contains the value of the stellar mass in solar units ( $M_*/M_{\text{sun}}$ ), the stellar luminosity in solar units ( $L_*/L_{\text{sun}}$ ), the effective temperature in Kelvin ( $T_{\text{eff}}[\text{K}]$ ), the age in  $10^6$  yr units ( $\text{Time}[1e6\text{yr}]$ ), and the asymptotic period spacing in seconds ( $\text{DPa}[\text{s}]$ ), computed as in Tassoul et al. (1990). Below the heading, the following quantities are listed: the harmonic degree ( $\ell$ ), the radial order ( $k$ ), the periods ( $\text{Period}$ ), the forward period spacings ( $\text{DP}$ ), the logarithm of the oscillation kinetic energies ( $\log(\text{Ek})$ ), and the first order rotation splitting coefficients ( $\text{C}_{k\ell}$ ).

A very important quantity such as the rate of period change of a given pulsation mode with radial order  $k$  ( $\dot{\Pi}_k \equiv d\Pi_k/dt$ ), can be easily computed from the age ( $\tau$ ) and the period ( $\Pi_k$ ) of a given model ( $j$ ) and the corresponding values of the previous model ( $j - 1$ ):

$$\frac{d\Pi_k}{dt} = \frac{\Pi_k^j - \Pi_k^{j-1}}{\tau^j - \tau^{j-1}}$$

Finally, we also give the option of downloading the *complete* set of periods (for all stellar masses, H envelopes and effective temperatures) at once in the hyperlink below the table.

#### 4.2. The second table: periods and other quantities for $\ell = 2$

All the above explanation holds also for the case of the second table, but in this case, the results correspond to  $\ell = 2$  pulsation modes.

#### 4.3. The third table: critical frequencies and chemical profiles

Now, if you click (for instance) at element [-3.62](#) in the first column of the table, you will download the file: `par001_0.525_3.623.tgz`. Again, this file corresponds to the sequence with  $M_* = 0.525M_{\odot}$  and  $\log(M_{\text{H}}/M_*) = -3.623$ . After you detar the file, you should obtain a sequence of files:

```
par001_0.525_3.623.out
par002_0.525_3.623.out
par003_0.525_3.623.out
par004_0.525_3.623.out
⋮
```

Again, each of these files correspond to a different, decreasing effective temperature. But, at variance with the cases of the first and second tables, in this case the interval in  $T_{\text{eff}}$  between consecutive files is quite large ( $\sim 500$  K). In Fig. 4 we show the appearance of the file `par001_0.525_3.623.out`. The parameters at the heading are, in this case, the stellar mass, the stellar luminosity, and the effective temperature. Below the heading, the following quantities are listed: the normalized radial coordinate, ( $r/R_{\text{sun}}$ ), the outer mass fraction coordinate ( $-\log q$ ), the squared Brunt-Väisälä frequency ( $N^2$ ), the squared Lamb frequency ( $L^2$ ), the Ledoux term ( $\text{BLedoux}$ ), and finally the abundance by mass of hydrogen (H1), helium (He4), carbon (C12), and oxygen (O16).

```

# M */M_sun      Teff[K]      L */L_sun
# 0.525          13933.474    0.72195098E-02

# r/R_sun      -log q      N^2      L^2      B Ledoux      H1      He4      C12      O16
0.1000E+01    0.1473E+02  0.9187E+02  0.2233E-04  0.0000E+00  0.9968E+00  0.9896E-07  0.9943E-07  0.9970E-07
0.1000E+01    0.1472E+02  0.9220E+02  0.2249E-04  0.0000E+00  0.9968E+00  0.9896E-07  0.9943E-07  0.9970E-07
0.1000E+01    0.1471E+02  0.9254E+02  0.2264E-04  0.0000E+00  0.9968E+00  0.9896E-07  0.9943E-07  0.9970E-07
0.1000E+01    0.1470E+02  0.9287E+02  0.2280E-04  0.1632E-22  0.9968E+00  0.9896E-07  0.9943E-07  0.9970E-07
0.1000E+01    0.1469E+02  0.9321E+02  0.2296E-04  0.0000E+00  0.9968E+00  0.9896E-07  0.9943E-07  0.9970E-07
0.1000E+01    0.1468E+02  0.9355E+02  0.2311E-04  0.0000E+00  0.9968E+00  0.9896E-07  0.9943E-07  0.9970E-07
0.1000E+01    0.1466E+02  0.9389E+02  0.2327E-04  0.0000E+00  0.9968E+00  0.9896E-07  0.9943E-07  0.9970E-07
0.1000E+01    0.1465E+02  0.9423E+02  0.2342E-04  0.0000E+00  0.9968E+00  0.9896E-07  0.9943E-07  0.9970E-07
0.1000E+01    0.1464E+02  0.9458E+02  0.2357E-04  0.0000E+00  0.9968E+00  0.9896E-07  0.9943E-07  0.9970E-07
0.1000E+01    0.1463E+02  0.9493E+02  0.2372E-04  0.6545E-23  0.9968E+00  0.9896E-07  0.9943E-07  0.9970E-07
0.1000E+01    0.1462E+02  0.9528E+02  0.2387E-04  0.0000E+00  0.9968E+00  0.9896E-07  0.9943E-07  0.9970E-07
0.1000E+01    0.1461E+02  0.9561E+02  0.2401E-04  0.0000E+00  0.9968E+00  0.9896E-07  0.9943E-07  0.9970E-07
0.1000E+01    0.1460E+02  0.9594E+02  0.2416E-04  0.1113E-22  0.9968E+00  0.9896E-07  0.9943E-07  0.9970E-07
0.1000E+01    0.1459E+02  0.9625E+02  0.2430E-04  0.1969E-21  0.9968E+00  0.9896E-07  0.9943E-07  0.9970E-07
0.1000E+01    0.1458E+02  0.9654E+02  0.2445E-04  0.4300E-21  0.9968E+00  0.9896E-07  0.9943E-07  0.9970E-07
0.1000E+01    0.1457E+02  0.9682E+02  0.2459E-04  0.2052E-21  0.9968E+00  0.9896E-07  0.9943E-07  0.9970E-07
0.1000E+01    0.1456E+02  0.9707E+02  0.2472E-04  0.0000E+00  0.9968E+00  0.9896E-07  0.9943E-07  0.9970E-07
0.1000E+01    0.1455E+02  0.9731E+02  0.2486E-04  0.1244E-21  0.9968E+00  0.9896E-07  0.9943E-07  0.9970E-07
0.1000E+01    0.1453E+02  0.9752E+02  0.2500E-04  0.1639E-22  0.9968E+00  0.9896E-07  0.9943E-07  0.9970E-07
0.9999E+00    0.1452E+02  0.9771E+02  0.2513E-04  0.4732E-22  0.9968E+00  0.9896E-07  0.9943E-07  0.9970E-07
0.9999E+00    0.1451E+02  0.9788E+02  0.2526E-04  0.2823E-21  0.9968E+00  0.9896E-07  0.9943E-07  0.9970E-07
0.9999E+00    0.1450E+02  0.9802E+02  0.2539E-04  0.2234E-21  0.9968E+00  0.9896E-07  0.9943E-07  0.9970E-07
0.9999E+00    0.1449E+02  0.9814E+02  0.2552E-04  0.4611E-22  0.9968E+00  0.9896E-07  0.9943E-07  0.9970E-07
0.9999E+00    0.1448E+02  0.9823E+02  0.2565E-04  0.8099E-21  0.9968E+00  0.9896E-07  0.9943E-07  0.9970E-07
0.9999E+00    0.1447E+02  0.9830E+02  0.2578E-04  0.1374E-20  0.9968E+00  0.9896E-07  0.9943E-07  0.9970E-07
0.9999E+00    0.1446E+02  0.9835E+02  0.2590E-04  0.1294E-21  0.9968E+00  0.9896E-07  0.9943E-07  0.9970E-07
0.9999E+00    0.1445E+02  0.9841E+02  0.2603E-04  0.0000E+00  0.9968E+00  0.9896E-07  0.9943E-07  0.9970E-07
0.9999E+00    0.1444E+02  0.9852E+02  0.2616E-04  0.1146E-21  0.9968E+00  0.9896E-07  0.9943E-07  0.9970E-07
0.9999E+00    0.1443E+02  0.9863E+02  0.2630E-04  0.0000E+00  0.9968E+00  0.9896E-07  0.9943E-07  0.9970E-07
0.9999E+00    0.1441E+02  0.9874E+02  0.2643E-04  0.0000E+00  0.9968E+00  0.9896E-07  0.9943E-07  0.9970E-07
0.9999E+00    0.1440E+02  0.9884E+02  0.2656E-04  0.0000E+00  0.9968E+00  0.9896E-07  0.9943E-07  0.9970E-07
0.9999E+00    0.1439E+02  0.9893E+02  0.2669E-04  0.0000E+00  0.9968E+00  0.9896E-07  0.9943E-07  0.9970E-07
0.9999E+00    0.1438E+02  0.9901E+02  0.2682E-04  0.2080E-21  0.9968E+00  0.9896E-07  0.9943E-07  0.9970E-07
0.9999E+00    0.1437E+02  0.9908E+02  0.2695E-04  0.4521E-21  0.9968E+00  0.9896E-07  0.9943E-07  0.9970E-07
0.9999E+00    0.1436E+02  0.9914E+02  0.2708E-04  0.0000E+00  0.9968E+00  0.9896E-07  0.9943E-07  0.9970E-07

```

Figure 4. The aspect of the file `par001_0.525_3.623.out`, corresponding to a DA white dwarf model with  $M_* = 0.525M_\odot$ ,  $L_*/L_\odot = 7.22 \times 10^{-3}$ ,  $T_{\text{eff}} = 13933$  K, and  $\log(M_{\text{H}}/M_*) = -3.623$ .

## 5. Final remarks

- Additional results for other values of the H envelope thickness that are not included in this database, can be obtained by request to the authors.
- If you use this database and publishes your results, please cite the paper: “*Toward ensemble asteroseismology of ZZ Ceti stars with fully evolutionary models*”, Romero, A. D., Córscico, A. H., Althaus, L. G., Kepler, S. O., Castanheira, B. G., Miller Bertolami, M. M. 2012, MNRAS, 420, 1462
- Any comment/criticism that helps to improve this database will be greatly appreciated!

## References

- Alexander, D. R., & Ferguson, J. W. 1994, ApJ, 437, 879
- Althaus, L. G., Córscico A. H., García-Berro, E., & Isern, J. 2010a, A&AR, 18, 471
- Althaus, L. G., Córscico, A. H., Bischoff-Kim, A., Romero, A. D., Renedo, I., García-Berro, E., & Miller Bertolami, M. M. 2010b, ApJ, 717, 897
- Angulo, C., et al. 1999, Nuclear Physics A, 656, 3
- Burgers, J. M. 1969, “*Flow Equations for Composite Gases*”, New York: Academic Press
- Cassisi, S., Potekhin, A. Y., Pietrinferni, A., Catelan, M., & Salaris, M. 2007, ApJ, 661, 1094
- Córscico, A. H., Althaus, L. G., Miller Bertolami, M. M., & García-Berro, E. 2009, A&A, 499, 257
- Córscico, A. H., Althaus, L. G., Kepler, S. O., Costa, J. E. S., & Miller Bertolami, M. M. 2008, A&A, 478, 869
- Córscico, A. H., Althaus, L. G., Miller Bertolami, M. M., & Werner, K. 2007a, A&A, 461, 1095
- Córscico, A. H., Miller Bertolami, M. M., Althaus, L. G., Vauclair, G., & Werner, K. 2007b, A&A, 475, 619
- Córscico, A. H., & Althaus, L. G. 2006, A&A, 454, 863
- Dziembowski, W. 1971, Acta Astron., 21, 289
- Haft, M., Raffelt, G., & Weiss, A. 1994, ApJ, 425, 222
- Iglesias, C. A., & Rogers, F. J. 1996, ApJ, 464, 943
- Itoh, N., Hayashi, H., Nishikawa, A., & Kohyama, Y. 1996, ApJS, 102, 411
- Magni, G., & Mazzitelli, I. 1979, A&A, 72, 134
- Renedo, I., Althaus, L. G., Miller Bertolami, M. M., Romero, A. D., Córscico, A. H., Rohrmann, R. D., & García-Berro, E. 2010, ApJ, 717, 183
- Romero, A. D., Córscico, A. H., Althaus, L. G., Kepler, S. O., Castanheira, B. G., & Miller Bertolami, M. M. 2012, MNRAS, 420, 1462
- Romero, A. D. 2012, PhD Thesis, Universidad de Buenos Aires
- Salaris, M., Dominguez, I., García-Berro, E., Hernanz, M., Isern, J., & Mochkovitch, R. 1997, ApJ, 486, 413
- Segretain, L., Chabrier, G., Hernanz, M., García-Berro, E., Isern, J., & Mochkovitch, R. 1994, ApJ, 434, 641
- Tassoul, M., Fontaine, G., & Winget, D. E. 1990, ApJS, 72, 335
- Unglaub, K., & Bues, I. 2000, A&A, 359, 1042
- Unno, W., Osaki, Y., Ando, H., Saio, H., & Shibahashi, H., 1989, “*Nonradial Oscillations of Stars*”, University of Tokyo Press, 2nd edition
- Winget, D. E., & Kepler, S. O., 2008, ARAA, 46, 157